Clays and Clay Minerals, Vol. 36, No. 6, 505–520, 1988.

HYDROTHERMAL AND SUPERGENE ALTERATIONS IN THE GRANITIC CUPOLA OF MONTEBRAS, CREUSE, FRANCE

P. DUDOIGNON, D. BEAUFORT, AND A. MEUNIER

Université de Poitiers, U.F.R. Sciences, Laboratoire de pétrologie des altérations hydrothermales
E.R.A. 220 du C.N.R.S., 40, Avenue du recteur Pineau
86022 Poitiers Cedex, France

Abstract—A mineralogical investigation of the highly kaolinized Chanon granite and albite-muscovite granite of the Montebras cupola, Creuse, France, indicates that the magmatic stage was followed by two hydrothermal events related to successive cooling stages and by late weathering. The hydrothermal alteration was accompanied first by greisen formation and then a broad kaolinization process, which pervasively affected the granitic bodies. In the Chanon granite, the greisens are characterized by a trilithionite-lepidolite-quartz-tourmaline assemblage and are surrounded by concentric alteration zones. From the greisen to the fresh granite three zones were distinguished: (1) a zone characterized by secondary brown biotite (<400°C), (2) a zone characterized by secondary green biotite and phengite (300–350°C), and (3) a zone characterized by the presence of corrensite (180°–200°C) located around greisen veinlets. In the albite-muscovite granite the greisen is composed of lepidolite and quartz. This mineral assemblage was followed locally by Li-tosudite crystallization. During the second hydrothermal event (<100°C) an assemblage of kaolinite, mixed-layer illite/smectite (I/S), and illite formed pervasively and in crack fillings; the smectite layers of the I/S are potassic. Weathering produced Fe oxide and kaolinite. This kind of alteration developed mainly in the overlying Chanon granite. Here, Ca-Mg-montmorillonite formed in subvertical cracks, which transect the two granitic bodies, and hydrothermal I/S was obliterated by Ca-Mg-montmorillonite.

The hydrothermal parageneses were apparently controlled by magmatic albitization and the bulk chemistry of the two granitic bodies. The albitization, the formation of large micaceous greisens, and the successive recrystallizations of biotite (which was the most susceptible phase to alteration) provide information on the temperature range and chemical mobility during successive cooling stages. Si and Mg activities increased as the temperature of alteration decreased, and secondary Mg-biotite and Mg-phengite crystallized as long as the K activity was sufficient. The crystallizations of secondary biotite and phengite were followed by the crystallization of I/S during stages of low K activity. Secondary hydrothermal phases in the Chanon granite contain substantial Fe and Mg. Secondary hydrothermal phases in the albite-muscovite granite contain only small amounts of Fe and Mg, suggesting a lack of chemical exchange between the enclosing Chanon granite and the albite-muscovite granite, which is depleted in Fe-Mg-rich primary phases, such as biotite.

Key Words—Biotite, Chlorite, Corrensite, Granite, Greisen, Hydrothermal, Kaolin, Petrography, Weathering.

INTRODUCTION

The general mechanisms of alteration of highly kaolinized granites have been extensively described (Nicolas and Rosen, 1966; Charoy, 1975; Exley, 1976; Konta, 1969). Both hydrothermal and supergene processes have been invoked to explain the formation of the kaolinite, but no conclusive evidence that allows a choice to be made between these two possible origins has arisen, despite the great temperature difference between greisen formation and near-surface conditions. The chief problem, of course, is to ascertain what happened during the cooling of a granite from the high-temperature hydrothermal event until the supergene alteration event. Occurrences of superimposed hydrothermal and supergene alterations were recently recorded for granites (Meunier and Velde, 1982; Dudoignon, 1983; Cathelineau, 1982); these authors concluded that clay minerals produced by hydrothermal or supergene alterations could be distinguished by the nature of their interlayer cations, i.e., potassic for the hydrothermal clay minerals and calcic for the supergene clay minerals.

The granitic cupola of Montebras, Creuse, France, is highly kaolinized, but shows several types of altered rock in which different secondary mineral assemblage can be identified. Three alteration episodes may be plausibly invoked for the alteration of the granitic bodies, i.e., high-temperature hydrothermal alteration related to greisen formation, late-stage hydrothermal alteration, and present-day weathering. Each alteration episode was accompanied by specific alteration conditions during the cooling of the granite and produced different clay minerals from the parent rocks (Meunier, 1982; Beaufort and Meunier, 1983a, 1983b; Beaufort, 1984). The present investigation was designed to identify and characterize the different parageneses so that their specific origins in the chronology of the different hydrothermal episodes could be identified and their

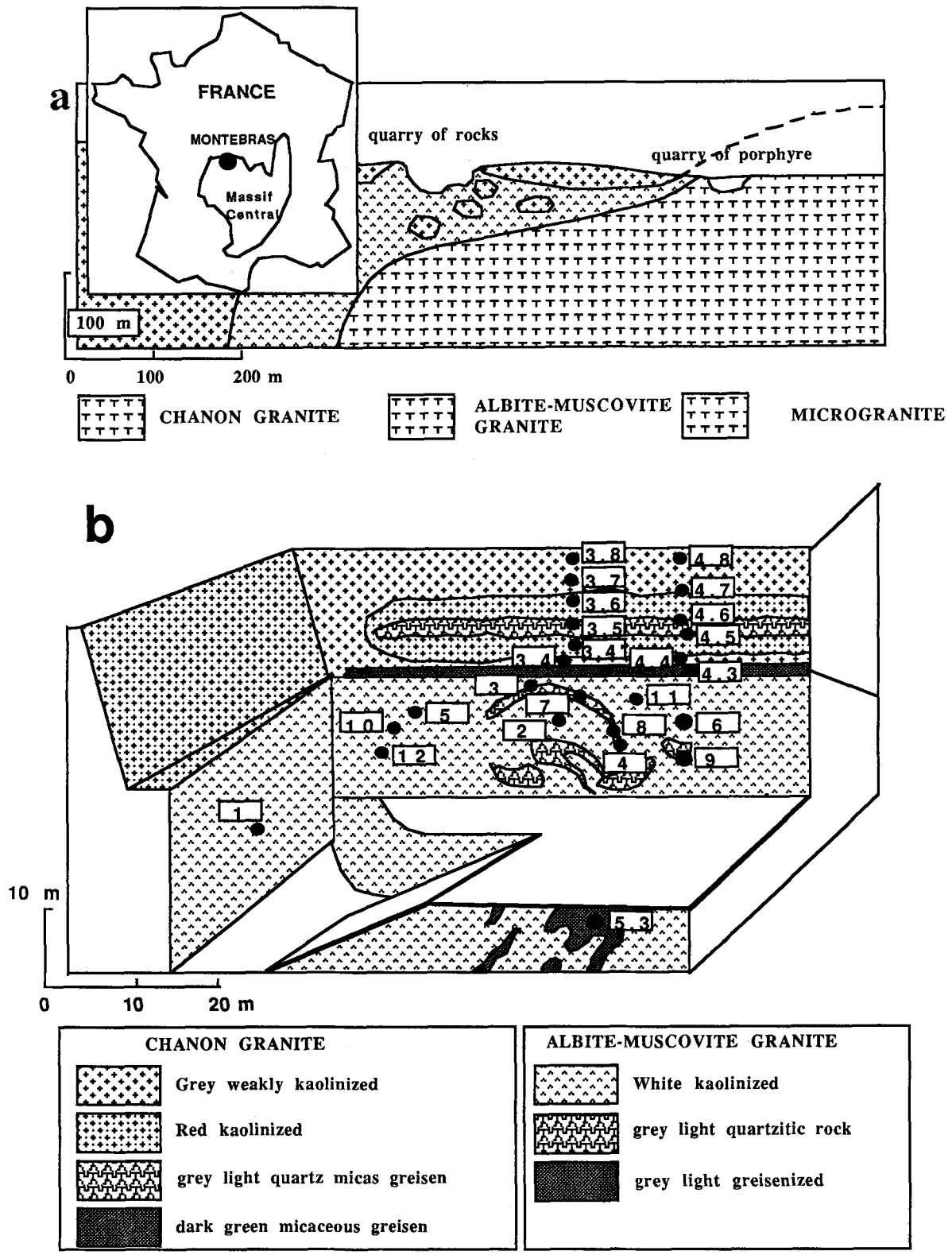

Figure 1. (a) Location map and east–west schematic cross section of Montebras cupola (Aubert, 1969). (b) Schematic representation of the northwest corner of the "quarry of rocks" showing sample locations.

https://doi.org/10.1346/CCMN.1988.0360604 Published online by Cambridge University Press

Table 1. Macroscopic characteristics of samples studied from Montebras Chanon granite and albite-muscovite granite.

Samples	Description	Plagioclase	K-feldspar	Biotite	Veins and veinlets
		Chanon granite			
3.7, 3.8, 4.8	grey, weakly kaolinized, porphyritic two-mica granite	weakly kaolinized	unaltered	unaltered	subvertical veins filled with white clay minerals or pale-green clay minerals
3.6, 4.7	red, kaolinized, friable granite	red, kaolinized	unaltered	red, kaolinized	greisen vein surrounded by greisenized granite and successive alteration zones
3.5, 4.6	grey, light-colored quartz-mica-tourmaline greisen	obliterated	obliterated	obliterated	
3.4′	greisenized, weakly kaolinized, two-mica granite	obliterated	obliterated	replaced by white micas	
4.5	red, kaolinized, friable granite	red, kaolinized	unaltered	red, kaolinized	greisen vein surrounded by greisenized granite and successive alteration zones
3.4, 4.4	grey, weakly kaolinzed, porphyritic two-mica granite	weakly kaolinized	unaltered	unaltered	greisen vein surrounded by greisenized granite and successive alteration zones
4.3	dark-green, micaceous, monomineralic greisen	obliterated	obliterated	replaced by white micas	
		Albite-muscovite granite			
5, 6, 7, 8, 9	weakly kaolinized, albite-muscovite granite	unaltered or weakly kaolinized	unaltered	unaltered	large veins filled with light-green micaceous material
10, 11, 12	white, kaolinized, friable granite, locally red-colored by iron oxides	kaolinized	unaltered or weakly kaolinized	unaltered	light-green, micaceous veins containing fluorapatite
2, 3, 4, 05, 3	light-green, greisenized, mica-rich granite	obliterated	unaltered or weakly kaolinized	obliterated	veins filled with white clay minerals
1	light-grey, quartzitic rock	obliterated	obliterated	unaltered	

relationship to the thermal history of the granite cupola determined.

GEOLOGICAL SETTING

The granitic cupola of Montebras was described by Aubert (1969). It is located in the northern part of a complex granitic body, which is elongated in an east–west direction and which is intruded between the metamorphic formations of Aigurande in the north and of Lepaud in the south. The cupola is composed of four distinct units observable in two quarries ("quarries of porphyries" and "quarry of rocks"; Figure 1a): (1) a central cupola of microgranite; (2) a capping albite-muscovite granite surrounding the microgranite; (3) an enclosing two-mica granite, called "Chanon granite", which is cut by

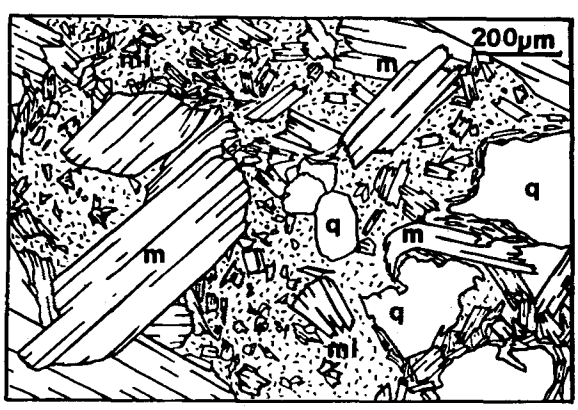

Figure 2. Sketch of light-green, micaceous greisen in albite-muscovite granite. m = large flakes of muscovite and lepidolite; mi = microcrystalline micaceous matrix; q = quartz.

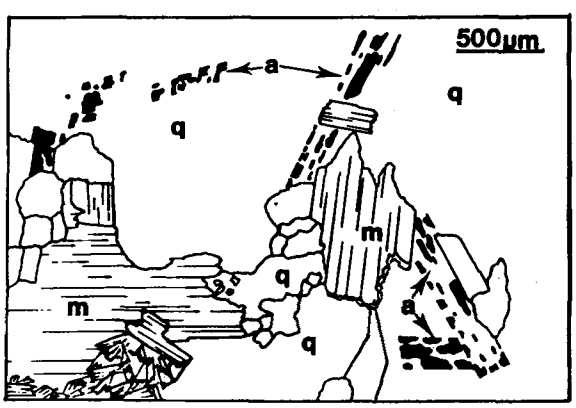

Figure 3. Sketch showing invasion or replacement of primary muscovite (m) and albite by large quartz crystals (q). Shapes of dissolved albite (a) are outlined by numerous aligned vesicles.

https://doi.org/10.1346/CCMN.1988.0360604 Published online by Cambridge University Press

Figure 4. Sketch showing light-grey, quartz-micaceous greisen in the Chanon granite. Primary muscovite (m) is recrystallized into flakes of lithian micas (mi). Biotite is replaced by protolithionites, which occlude needles of rutile. Quartz crystals are invaded by a microcrystalline lepidolitic matrix. t = acicular tourmaline.

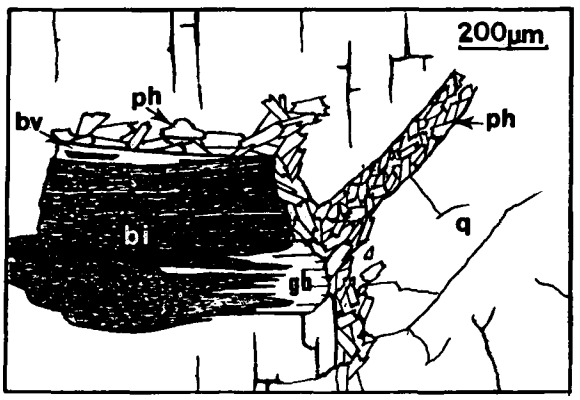

Figure 5. Sketch showing small phengite (ph) grains crystallized in veinlets and at contact in biotite (bi) in intergranular joints. Brown biotite (bv) shows peripheral green biotite (gb) recrystallizations.

quartz veins and aplitic dikes emerging from the cupola; and (4) greisen, typical pegmatitic, feldspathic, and quartzitic ("stockscheider" and "quartzglocke") bodies, which replace the Chanon granite along its contact with the albite-muscovite body.

These units are highly altered in the "quarry of rocks" from which kaolin is mined. Contacts between the albite-muscovite granite and the enclosing Chanon granite are outlined by a pegmatite body. The fresh albite-muscovite granite is a light grey, sugary to granular rock. Its average grain size is 1 mm; its modal analysis is: quartz 20–30%, K-feldspar 15–30%, albite 30–50%, muscovite 5–10%, and apatite, topaz, cassiterite, and niobo-tantalite ($(Fe,Mn)(Nb,Ta)_2O_6$) <1% (Aubert, 1969). Three different types of alteration products have been observed: (1) a light-green micaceous, monomineralic type of greisen, (2) light-grey quartzitic assemblage, which is locally red, and (3) a white kaolinized granite. The Chanon granite is a porphyritic two-mica granite characterized by K-feldspar phenocrysts about 4 cm in size and by centimeter-size primary cordierite grains, which have been entirely replaced by biotite. Its modal composition is: quartz 28.6%, K-feldspar 21.30%, plagioclase 28.20%, muscovite 4.20%, and biotite 13.50%.

Four different types of alteration products have been noted for the Chanon granite: (1) a dark-green, micaceous, monomineralic greisen at the contact with the underlying albite-muscovite granite; (2) a light-grey greisen rich in quartz, mica, and tourmaline; (3) a red, kaolinized, friable granite enclosing the greisens; and (4) a grey, weakly kaolinized granite, which replaces the fresh rock on the major part of the working face (Figure 1b).

METHOD OF INVESTIGATION

Twelve samples were collected along two vertical profiles in the Chanon granite plus twelve samples of the different alteration products in the albite-muscovite granite. Veins and veinlets in the two granites were also sampled (Table 1, Figure 1b).

Secondary minerals were located in thin sections using a transmitted light microscope and then analyzed *in situ* with a Cameca MS 46 electron microprobe equipped with an EDS Si-Li detector (ORTEC). A very low energy electron beam was needed to avoid the destruction of these phases during counting (Velde, 1984). Analytical conditions were as follows: 15 kV, 0.001 µA, 120-s counting time, 3-µm spot size. After microprobe analyses, secondary minerals were extracted from

Table 2. Bulk-rock chemical analysis of the Chanon granite and albite-muscovite granite.

	Albite-muscovite granite												
	Greisenized granite						Quartzified granite				Kaolinized granite		
Sample	1	2	3	4	05-3	5	6	7	8	9	10	11	12
SiO_2	82.50	47.12	43.14	52.53	46.19	52.51	70.12	87.61	92.69	93.11	84.82	89.98	86.96
Al_2O_3	10.61	35.55	39.25	32.66	38.42	32.07	19.37	7.98	4.86	3.27	10.96	6.28	8.53
MnO	0.03	0.08	0.07	0.10	0.08	0.06	0.05	0.11	0.02	0.02	0.03	0.02	0.02
MgO	0.04	0.26	0.23	0.28	0.18	0.16	0.16	0.09	0.07	0.04	0.04	0.05	0.07
CaO	0.14	0.19	0.11	0.11	0.16	0.09	0.16	0.12	0.10	0.08	0.08	0.12	0.19
Na_2O	2.11	0.13	0.17	0.16	0.36	0.97	0.08	0.07	0.07	0.08	0.13	0.16	0.27
K_2O	3.48	8.26	9.94	8.37	7.23	8.46	3.77	1.58	1.01	0.91	1.34	0.93	0.94
TiO_2	0	0.02	0	0	0	0	0	0	0	0	0	0	0
Li_2O	0	0.50	0.31	0.56	0.32	0.06	0.08	0.08	0	0	0	0.33	0.09
H_2O	1.02	6.62	5.33	5.23	6.80	4.43	4.38	1.65	1.04	0.53	3.12	1.79	2.61
Fe_2O_3	0.09	0.33	0.31	0.36	0.26	0.27	0.21	0.18	0.12	0.11	0.11	0.12	0.13
Total	100.02	99.06	98.76	100.36	100.0	99.01	98.38	99.47	99.98	98.15	100.63	99.78	99.81

Σ Fe as Fe_2O_3.

https://doi.org/10.1346/CCMN.1988.0360604 Published online by Cambridge University Press

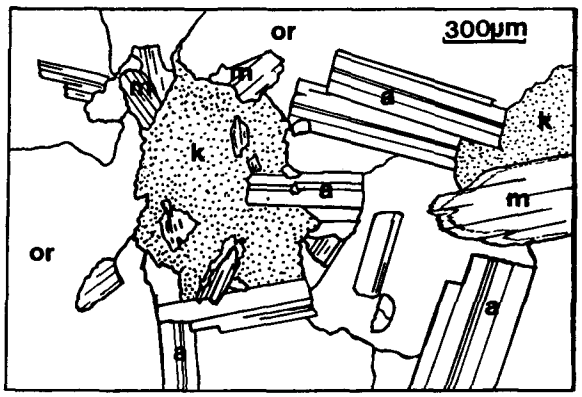

Figure 6. Sketch showing colorless cryptocrystalline matrix (K) invading the K-feldspar (or) and primary muscovite (m) in the white, kaolinized, albite-muscovite granite. a = albite.

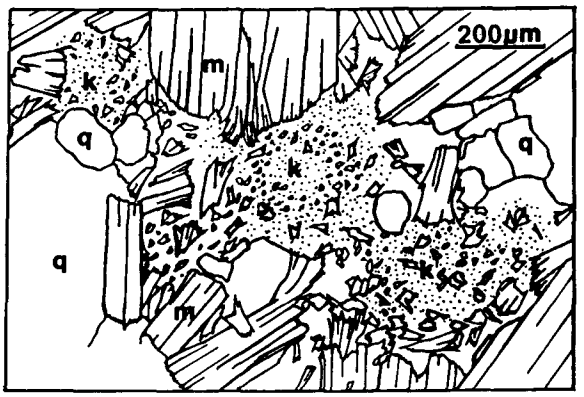

Figure 7. Sketch showing greisen in the albite-muscovite granite. Microcrystalline micaceous matrix is largely replaced by the colorless cryptocrystalline matrix (K). Large white mica flakes (m) are altered on their rims. q = quartz.

the thin sections using a microdrill (Beaufort *et al.*, 1983). X-ray powder diffraction patterns were obtained with a step-scan X-ray diffractometer (Philips PW 1730, 40 kV, 40 mA, CoKα radiations, steps of 0.1°2θ, count rate of 400 s/step) interconnected with an Apple II microcomputer for data storage. The percentage of smectite layers in mixed-layer clay minerals was determined by the Reynolds' method (1980). Bulk-rock chemical analyses obtained with an atomic absorption spectrophotometer (Perkin-Elmer 107) are listed in Table 2. Infrared spectra were recorded using KBr disks (0.5 mg of specimen in 300 mg of KBr) on a Beckmann IR 4240 spectrophotometer in the 4000–300-cm^{-1} frequency region.

PETROGRAPHY OF ALTERED ROCKS

Greisen in the albite-muscovite granite

The micaceous greisen in the albite-muscovite granite is a light-green rock composed of large flakes of muscovite and lepidolite (100–400 μm in size), randomly dispersed in a fine-grained micaceous matrix (20–50 μm in size) (Figure 2). Locally, muscovite, lepidolite, K-feldspar, and albite are invaded by large quartz crystals, which may completely engulf them (quartzitic facies). Numerous aligned vesicles preserve the arrangement and shape of original feldspar crystals after replacement (Figure 3). Some millimeter-size veinlets are present at the contact between the quartzitic facies and the micaceous facies; the veinlets are filled with black manganese oxides and some gorceixite.

Greisen in the Chanon granite

A dark-green greisen occurs in the Chanon granite along its contact with the albite-muscovite granite. It obliterates the initial microstructure of the two-mica granite, preserving only the shapes of the altered cordierite phenocrysts. Microscopically, the rock is similar to the light-green greisen in the albite-muscovite granite, but the large grains of trilithionites show a weak, yellow-brown pleochroism and inner microrecrystallizations.

In the upper quartz- and tourmaline-rich greisen pri-

Table 2. Continued.

Chanon granite											
Section 1						Section 2					
03.8	03.7	03.6	03.5	03.4'	03.4	04.8	04.7	04.6	04.5	04.4	04.3
75.71	71.82	74.31	76.80	73.03	74.03	62.28	66.29	84.41	66.11	63.61	46.48
12.43	15.11	15.21	11.85	13.50	13.62	21.06	19.33	8.08	17.99	19.76	28.41
0.03	0.04	0.02	0.05	0.10	0.03	0.08	0.03	0.08	0.04	0.03	0.18
0.78	1.04	0.63	0.66	1.11	0.43	1.75	0.85	0.50	1.02	0.79	1.33
0.68	0.51	0.27	0.17	0.11	0.21	0.24	0.15	0.18	0.15	0.11	0.18
2.31	2.12	0.22	0.18	0.18	0.22	0.26	0.14	0.09	0.59	0.23	0.19
3.01	4.71	2.95	4.05	4.58	1.90	4.61	3.90	3.24	5.93	6.08	10.41
0.10	0.10	0.26	0.10	0.18	0.25	0.63	0.52	0.19	0.44	0.39	0.02
0	0	0	1.09	2.28	0	0.02	0	0.91	0	0	3.38
1.72	1.83	4.57	2.03	2.70	4.72	5.55	5.96	1.47	4.31	4.82	3.94
2.07	2.52	2.16	1.48	2.76	2.23	3.73	2.73	1.13	2.68	2.24	3.38
98.94	99.80	98.50	98.46	100.53	97.64	100.21	99.26	100.28	99.26	98.06	98.18

https://doi.org/10.1346/CCMN.1988.0360604 Published online by Cambridge University Press

Table 3. Atomic ratio of dark-green, micaceous, monomineralic greisen (Chanon granite/albite muscovite granite contact).

	A	B
Si	3.27	3.14
Al^{IV}	0.73	0.86
Al^{VI}	1.63	1.40
Mg	0.14	0.13
Fe^{2+}	0.18	0.17
Ti	0.00	0.00
Mn	0.01	0.01
Li	n.d.	0.92
Σ oct	1.96	2.63
Ca	0.01	0.01
Na	0.03	0.02
K	0.94	0.90

A = structural formula calculated on the basis of 11 oxygens (Li not included).

B = structural formula calculated on the basis of 11 oxygens (including Li).

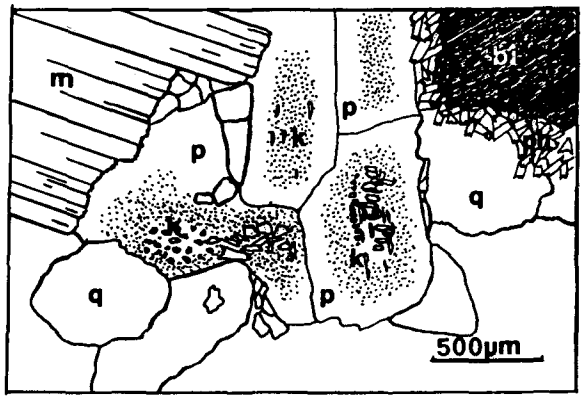

Figure 8. Sketch showing inner part of plagioclases (p) recrystallized into colorless phyllosilicates and cryptocrystalline matrix (K). Phengites (ph) located around biotites (bi) are altered.

mary muscovite and feldspar have been replaced by thin flakes of lithian muscovite. Primary biotite is recrystallized to colorless or weakly pleochroic trilithionite, which occludes numerous sagenite-twinned rutile crystals. This recrystallized biotite is locally surrounded by white secondary mica. The large quartz crystals have been replaced by a microcrystalline lepidolitic matrix along their contact with muscovite or biotite grains (Figure 4). Two types of tourmaline are present: (1) green acicular crystals occluded in quartz phenocrysts and (2) globular crystals, in the micaceous matrix. The altered tourmaline is zoned, brown in the core, and blue in the rim; most are invaded by microcrystalline mica.

Alteration zones surrounding the quartz-tourmaline greisen

This upper quartz-tourmaline greisen is a massive body surrounded by two different alteration zones. In the nearer zone (0.5–1.0-m thick), primary biotite has partly or entirely recrystallized to secondary brown biotite, <50 µm in size. Secondary biotite invades neighboring minerals along microcracks and intergranular joints. The farther zone (1.0–2.0-m thick) is characterized by small phengite flakes in veinlets and intergranular joints and by green biotite replacing primary and secondary brown biotite (Figure 5).

Illite-kaolinite and illite/smectite (I/S) mixed-layer alteration products

Altered rocks are friable and white. In the albite-muscovite granite, muscovite and K-feldspar are invaded or entirely replaced by a colorless clay matrix of illite-kaolinite-illite/smectite (I/S) (Figure 6). In the greisen in the albite-muscovite granite the microcrystalline mica is largely altered to a clay matrix, whereas large flakes of mica have recrystallized only on their rims; the bright polarization colors of the micaceous phases are gradually replaced by the grey polarization colors of kaolinite (Figure 7). In the Chanon granite this type of alteration has formed chiefly in the farther

Table 4. Microprobe analyses of muscovite and lepidolite from albite-muscovite granite.

	Muscovites						Lepidolites					
Si	3.10	3.03	3.14	3.06	3.08	3.12	3.61	3.64	3.58	3.67	3.76	3.68
Al^{IV}	0.90	0.97	0.86	3.94	0.92	0.88	0.39	0.36	0.42	0.33	0.24	0.32
Al^{VI}	1.96	1.96	1.95	1.95	2.01	1.97	1.59	1.58	1.75	1.63	1.55	1.58
Mg	—	—	—	—	—	—	—	—	—	—	—	—
Fe	0.05	0.04	0.04	0.04	0.02	0.03	0.23	0.19	0.11	0.21	0.27	0.28
Ti	—	—	0.01	—	—	—	—	—	—	—	—	—
Mn	—	0.01	0.02	—	—	—	0.13	0.11	0.05	0.04	0.03	—
Ca	—	—	—	0.01	0.00	0.03	—	—	—	—	—	0.01
Na	0.05	0.09	0.09	0.02	0.04	0.03	0.07	0.13	0.04	0.09	0.07	0.07
K	0.85	0.90	0.76	0.96	0.81	0.86	0.85	0.87	0.80	0.85	0.92	0.93
Σ oct	2.01	2.01	2.02	1.99	2.03	2.01	1.95	1.88	1.91	1.88	1.85	1.86

Calculated on the basis of 11 oxygens. Lithium is not counted in these analyses, and Li-rich micas are identified by their high Si atom contents and their octahedral occupancies of <2. Fe = Fe^{2+}.

https://doi.org/10.1346/CCMN.1988.0360604 Published online by Cambridge University Press

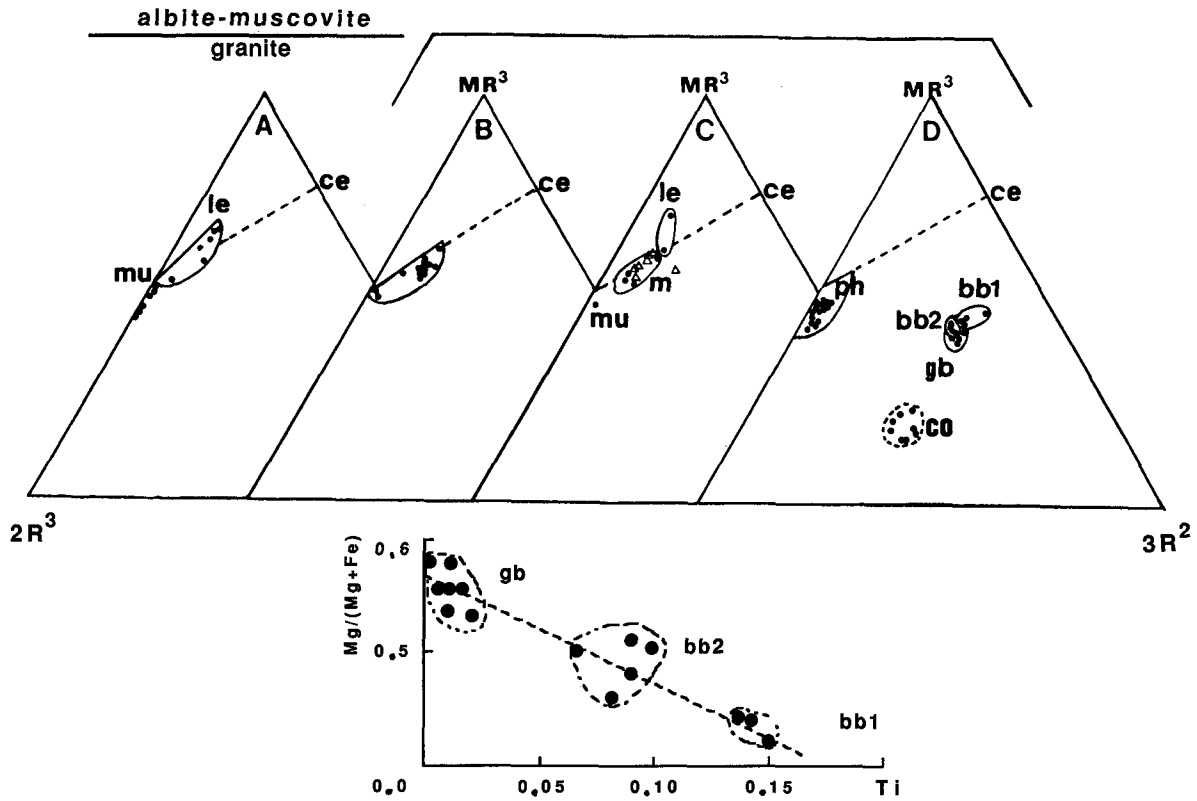

Figure 9. Chimiographic representation of analyzed micaceous phases in the MR^3-$2R^3$-$3R^2$ coordinates of (A) muscovites (mu) and lepidolites (le) in the albite-muscovite granite (Table 4), (B) lithian micas in the dark-green greisen in the Chanon granite (Table 6), (C) lithian micas in the light-grey greisen in the Chanon granite (Table 5): le = microcrystalline lepidolite, m = large lepidolite (circles) and protolithionite (triangles), mu = muscovite, (D) phengite (ph), primary biotite (bb1), secondary brown biotite (bb2), secondary green biotite (gb) and corrensite (co), (lower diagram) representation of biotite in Mg/(Mg + Fe) vs. Ti coordinates.

greisen, but it has also been superimposed on the green biotite-phengite alteration products. The interiors of plagioclase grains are partly replaced (Figure 8) and recrystallized to a white, cryptocrystalline matrix. Primary and secondary micaceous phases show recrystallized outer rims; their cleavages are sinuous, and grey polarization colors replace bright primary colors. The inner parts of cordierite grains have been recrystallized to kaolinite, which includes some relict grains of secondary green biotite and phengite.

Tosudite alteration type

The fresh albite-muscovite granite sampled on the wall rock in the western part of the quarry is pervasively altered. All primary minerals have been invaded and partly replaced by colorless, clay-size flakes of tosudite (about 20 μm in size), which display grey polarization colors. Muscovite appears to be the least altered primary mineral.

Kaolinite-iron oxide alteration products

Most of the Chanon granite, except the greisen, is extensively kaolinized. The quartzitic facies of the albite-muscovite granite has also been kaolinized. In the red, kaolinized Chanon granite biotite has been pseudomorphically replaced by kaolinite. This replacement appears to have started along intergranular joints, whereas some relict biotite recrystallized to a biotite/vermiculite mixed-layer mineral. Iron oxides are present along intergranular joints and inside porous grains of kaolinized plagioclase.

Veins and veinlets

Two types of veins and veinlets were observed: (1) 1–5-cm-wide veins of greisen emerging from the upper greisen in the Chanon granite, and (2) 1-mm-wide to 1-cm-wide clayey veins in both the Chanon and the albite-muscovite granites. The first type of vein is surrounded by a 2-cm-wide alteration zone similar to those observed around the upper greisen; the green biotite, however, is replaced by corrensite. The second type of vein, as found in the Chanon granite, contains the following mineral assemblages: (1) green veins: kaolinite, illite, pure smectite; (2) white veins: illite, random I/S (45% smectite layers); (3) white veins: kaolinite, random I/S (50% smectite layers).

https://doi.org/10.1346/CCMN.1988.0360604 Published online by Cambridge University Press

Table 5. Microprobe analyses of micaceous phases from light-grey, quartz-mica greisenized Chanon granite.

	1	2	3	4	5	6	7	8	9	10	11	12	13	14	15	16	17
Si	3.02	3.29	3.14	3.52	3.48	3.64	3.70	3.40	3.37	3.41	3.43	3.47	3.48	3.45	3.50	3.61	3.59
Al^{IV}	0.98	0.71	0.86	0.48	0.52	0.36	0.30	0.60	0.63	0.59	0.57	0.53	0.52	0.55	0.50	0.39	0.41
Al^{VI}	1.90	1.68	1.65	1.49	1.53	1.46	1.46	1.04	1.26	1.54	1.55	1.63	1.50	1.62	1.60	1.49	1.55
Mg	0.08	0.14	0.19	0.19	0.20	0.21	0.22	0.18	0.28	0.17	0.19	0.17	0.20	0.12	0.12	0.16	0.19
Fe	0.07	0.14	0.14	0.32	0.18	0.23	0.22	0.14	0.58	0.22	0.22	0.17	0.25	0.26	0.24	0.30	0.18
Ti	–	0.01	0.02	–	0.01	0.01	0.02	0.01	0.02	0.02	0.01	0.01	0.01	–	0.01	0.01	0.01
Mn	0.01	0.01	0.01	0.01	–	0.03	0.02	0.01	0.03	0.02	0.02	–	0.02	0.01	0.01	0.02	0.01
Ca	–	–	–	0.02	–	0.01	–	–	–	–	–	–	–	0.01	–	–	–
Na	0.07	0.02	0.05	0.03	–	0.01	0.02	0.01	0	0.02	0.01	0.02	0.02	–	–	0.04	0.03
K	0.88	1.00	0.99	0.92	0.85	0.90	0.92	1.01	1.00	0.99	1.00	0.92	0.99	0.88	0.94	0.90	0.90
Σ oct	2.06	1.98	2.01	2.01	1.92	1.94	1.94	1.38	2.17	1.97	1.99	1.98	1.98	2.02	1.98	1.98	2.16

1 = recrystallized muscovite; 2–6 = small-size micaceous flakes; 7–8 = small-size micaceous flakes on quartz; 9–15 = large flakes of protolithionite and recrystallized biotites; 16–17 = small-size micaceous flakes on protolithionites.
Calculated on the basis of 11 oxygens. Fe = Fe^{2+}.

In the albite-muscovite granite the veins are filled with the following mineral assemblages: (1) green veins: illite, random I/S (40% smectite layers); (2) green veins: illite, kaolinite, random I/S (45% smectite layers); (3) red veins: illite, random I/S (57% smectite layers). Assemblages of green illite and I/S were also noted. Fluorapatite also occurs with the clay minerals in some assemblages.

COMPOSITIONS OF THE SECONDARY PHASES

Lithian micas

Li-rich phases are present in the micaceous greisen in the albite-muscovite granite (samples 2, 3, 4, 05-3, and 11) and in the two greisens in the Chanon granite (samples 03-5, 03-4, 04-6, and 04-3) (Table 1). Li-rich phyllosilicates were identified in thin sections by microprobe analyses despite the fact that Li was not measured. If analyses of Li-rich mica are calculated on a $O_{10}(OH)_2$ basis omitting Li, the Si content is overestimated and the octahedral occupancy is underestimated (Table 3). These properties were used to distinguish Li-rich phases from normal muscovites and biotites. On plotting their compositions on a MR^3-$2R^3$-$3R^2$ diagram (Velde, 1977, 1984, 1985), the MR^3 component was overestimated; hence, these minerals are clearly discriminated from muscovite-phengite or biotite solid solutions (Figure 9). In the greisen in the albite-muscovite granite, the mixture of $2M_1$ muscovite and lepidolite was evidenced both by XRD and microprobe analyses. The XRD patterns showed two *060* reflections at 1.495 Å (muscovite) and 1.525 Å (lepidolite) (Brindley and Brown, 1980; Monier, 1985). Microprobe analyses calculated on the basis of $O_{10}(OH)_2$ were distributed into two groups, true muscovites having octahedral occupancies ranging from 1.99 to 2.01 and low phengitic substitutions and Li-phases having lower octahedral occupancies and Si contents >3.00 (3.58–3.76). The low interlayer charges were probably due to admixture with small amounts of kaolinite (Table 4).

The trilithionites analyzed in the two greisens in the Chanon granite were identified by a 1.519-Å (060) XRD reflection instead of a 1.54-Å (060) reflection characteristic of biotite and by 002 and 020 reflection intensities that were intermediate between those of muscovite and biotite. Microprobe analyses showed Si contents of >3.37 and octahedral occupancies near 2.00 on an $O_{10}(OH)_2$ basis (Table 5). Lepidolite mica in the altered Chanon granite was characterized by a Si content of 3.20 to 3.70 (Tables 5 and 6) and a 1.525-Å (060) XRD reflection.

These micaceous phases are clearly distinct from muscovites or biotites on a MR^3-$2R^3$-$3R^2$ composition diagram; *their Li → Al octahedral substitutions* suggest a shift of their composition field towards the illite-phengite domain (Figure 9c).

https://doi.org/10.1346/CCMN.1988.0360604 Published online by Cambridge University Press

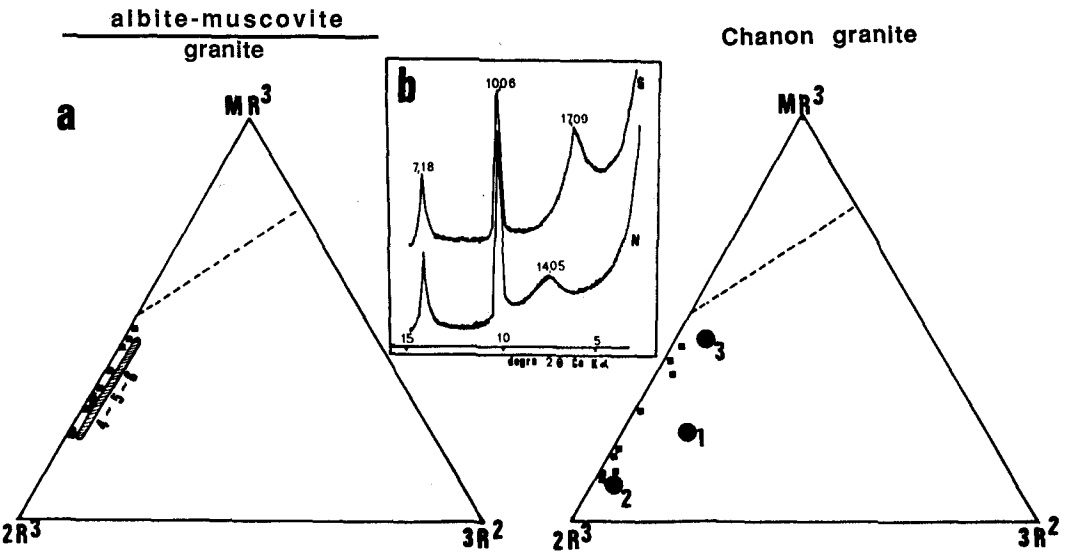

Figure 10. (a) Representation of the illite-kaolinite-illite/smectite (I/S) assemblages in the MR^3-$2R^3$-$3R^2$ coordinates. Squares = pervasive alteration (Tables 11 and 12); 4, 5, and 6 = vein fillings (albite-muscovite granite); 1, 2, and 3 = vein fillings (Chanon granite) (Table 13). (b) X-ray powder diffraction pattern of illite-kaolinite-random I/S assemblage pervasively crystallized during late hydrothermal event.

Phengites

Compositions of the phengitic micas in the weakly kaolinized Chanon granite, calculated on the basis of $O_{10}(OH)_2$, differ from those of muscovite by their Al → (Fe,Mg) octahedral substitutions, which range from 0.14 to 0.20. The phengites are magnesium-rich; the Mg/(Fe + Mg) atomic ratio ranges from 0.61 to 0.71. The smallest interlayer charges were probably due to some kaolinite admixture (Table 7, Figure 9d).

Biotites

The chemical compositions of the brown primary biotite, brown secondary biotite, and green biotite show several differences, especially in their Mg, Fe, and Ti contents. Atomic Mg/(Fe + Mg) ratios vs. Ti show a linear relation, with the lower Ti and higher Mg contents corresponding to secondary biotite. The average Mg/(Mg + Fe) atomic ratios vary from 0.42 for brown primary biotite to 0.49 for secondary biotite to 0.67 for green biotite, whereas the average Ti content decreases from 0.14 for the brown primary biotite to 0.085 for the brown secondary biotite and 0.02 for the green biotite (Table 8, Figure 9, lower).

Corrensite

Corrensite was identified on the basis of 14.65- and 29.28-Å XRD reflections on natural, oriented samples and 15.31- and 31.06-Å reflections after ethylene glycol treatment. The compositions listed in Table 9 appear to be the result of a mixture of residual biotite and ordered chlorite/smectite; the potassic interlayer charge ranges from 0.51 to 0.37, and the Mg/(Mg + Fe) atomic ratio ranges from 0.41 to 0.47. MR^3-$2R^3$-$3R^2$ plots of

Table 6. Microprobe analyses of lithian micas from dark-green greisen replacing Chanon granite at contact with albite-muscovite granite.

Si	3.38	3.47	3.54	3.46	3.56	3.51	3.55	3.12	3.49	3.57	3.49	3.38	3.20	3.59	3.64
Al^{IV}	0.62	0.53	0.46	0.54	0.44	0.49	0.45	0.88	0.51	0.43	0.51	0.62	0.80	0.41	0.36
Al^{VI}	1.70	1.55	1.56	1.56	1.55	1.55	1.46	1.88	1.54	1.47	1.56	1.72	1.85	1.52	1.53
Mg	0.13	0.15	0.16	0.19	0.17	0.22	0.17	0.08	0.16	0.19	0.16	0.13	0.12	0.18	0.17
Fe	0.13	0.23	0.25	0.28	0.24	0.24	0.30	0.05	0.30	0.34	0.27	0.17	0.06	0.28	0.25
Ti	0.01	0.01	0	0	0	0	0.02	0	0	0	0	0	0	0	0
Mn	0	0.02	0.02	0.01	0.01	0.01	0.02	0	0.02	0.01	0.02	0	0	0.01	0.01
Ca	0	0	0	0	0	0	0	0	0	0	0	0	0	0	0
Na	0.01	0.02	0.02	0.01	0.01	0.01	0.01	0.02	0	0.01	0.01	0.01	0.04	0.01	0.01
K	0.96	0.97	0.89	0.90	0.90	0.91	1.01	0.95	0.91	0.90	0.90	0.84	0.86	0.90	0.69
Σ oct	1.97	1.96	1.99	2.04	1.97	2.02	1.97	2.01	2.02	2.01	2.01	2.02	2.01	1.99	1.96

Calculated on the basis of 11 oxygens. Fe as Fe^{2+}.

https://doi.org/10.1346/CCMN.1988.0360604 Published online by Cambridge University Press

Table 7. Microprobe analyses of muscovites and phengites from weakly kaolinized Chanon granite.

	Muscovites								Phengites												
	5	6	7	8	9	10	11	12	13	12	13	14	15	16	17	18	19	20	21	22
Si	3.09	3.13	3.08	3.12	3.08	3.08	3.12	3.17	3.08	3.06	3.07	3.08	3.03	3.04	3.03	3.12	3.11	3.12	3.12	3.11
Al	2.85	2.79	2.83	2.77	2.84	2.83	2.81	2.80	2.89	2.83	2.81	2.81	2.91	2.88	2.91	2.74	2.76	2.71	2.73	2.72
Mg	0.02	0.02	0.02	0.02	0.02	0.02	0.02	0.02	0.02	0.10	0.11	0.11	0.10	0.11	0.10	0.11	0.11	0.12	0.12	0.13
Fe^{2+}	0.05	0.06	0.06	0.08	0.07	0.05	0.06	0.04	0.05	0.06	0.05	0.07	0.05	0.05	0.04	0.06	0.06	0.07	0.07	0.07
Ti	0.01	0	0.04	0.03	0.03	0.03	0.03	0.03	0	0	0	0.03	0.01	0.01	0.01	0.02	0.02	0.02	0.02	0.01
Mn	0	0.01	0	0	0	0	0	0	0.01	0	0	0	0	0	0	0	0	0	0	0
Ca	0	0	0	0	0	0	0	0	0	0	0	0	0	0	0.02	0	0	0	0	0
Na	0.05	0.05	0.07	0.08	0.05	0.06	0.04	0.03	0.05	0.10	0.06	0.07	0.07	0.06	0.04	0.05	0.05	0.04	0.05	0.08
K	0.88	0.91	0.84	0.87	0.05	0.85	0.82	0.70	0.83	0.84	0.89	0.79	0.75	0.78	0.78	0.84	0.83	0.90	0.87	0.86
Σ oct	2.02	1.99	2.01	2.00	1.99	1.99	2.02	2.04	2.03	2.05	2.04	2.10	2.10	2.10	2.09	2.05	2.06	2.04	2.06	2.04

Calculated on the basis of 11 oxygens. Fe as Fe^{2+}.

these chemical compositions are shifted from the biotite field towards the $2R^3$-$3R^2$ line (Table 9, Figure 9d).

Tosudite

Tosudite gave the characteristic XRD reflections of a regular mixed-layer dioctahedral chlorite/smectite: 30.15, 14.77, 9.08, 7.45, and 4.95 Å for natural, oriented samples and 30.87, 15.26, 7.76, and 5.15 Å for samples after ethylene glycol treatment and a 060 reflection at 1.490 Å. The structure collapsed to 12.18 Å on heating to 400°C, and only a weak 9.94-Å reflection persisted to 500°C. Tosudite was always mixed with a small amount of illite and kaolinite. IR spectra gave results similar to those obtained on Japanese tosudite samples analyzed by Ichikawa and Shimoda (1976), Sudo and Shimoda (1978), and Shimoda (1975). The 3630- and 3540-cm^{-1} absorption bands were assigned to OH valence vibrations in silicate and hydroxide layers; the 708-cm^{-1} band reflects the Mg-Al-OH grouping vibrations in hydroxide layer. Tosudite microprobe analyses are listed in Table 10; the following average structural formula was calculated on the basis of 50 oxygens and 1.60% Li_2O, as found by atomic absorption (Table 10, Creach *et al.*, 1986):

$$(Si_{14.13}Al_{2.47})^{IV}(Al_{11.08}Fe^{2+}_{0.09}Mg_{0.08}Mn_{0.07}Ti_{0.02}Li_{1.05})^{VI}$$
$$(Ca_{0.09}K_{0.79}Na_{0.18})O_{40}(OH)_{20}$$

Illite-kaolinite-random I/S assemblage

Illite, kaolinite, and random I/S are intimately mixed in the zones of pervasive alteration in the albite-muscovite granite, its greisen bodies, and in the Chanon granite. XRD patterns of natural, oriented samples show a 7.18-Å (001) kaolinite reflection, a 10.06-Å (001) mica reflection, and a 14.05-Å (001) reflection, which shifts to 17.09 Å after ethylene glycol treatment. This last peak can be attributed to a random I/S having 40% smectite layers (Figure 10b; Velde, 1985; Reynolds and Hower, 1970). Microprobe analyses show that the interlayer is mainly potassic and that the Si content <3.40. Al-for-Si substitutions suggest beidellite (Tables 11 and 12). Plotting these data on a MR^3-$2R^3$-$3R^2$ diagram yields compositional points in the same area, spread along the MR^3-$2R^3$ line from the illite to the kaolinite pole (Figure 10a).

The same mixture (illite-kaolinite-I/S) fills the veins and veinlets which cut the two granite bodies. The proportion of smectite layers in the I/S ranges from 40% to 90%. In the Chanon granite the smectite interlayer sites are calci-potassic; the Ca content ranges from 0.08 to 0.14, and the K content ranges from 0.08 to 0.29 (Table 13). The exchangeable ions of the more expandable mixed-layer clay are: 45.45 Ca^{2+}, 19.92 Mg^{2+}, 1.38 Na^+, and 1.41 K^+ meq/100 g vs. a cation-exchange capacity of 85 ± 8 meq/100 g. All these analyses show Al/Fe octahedral substitutions and, if plotted in MR^3-$2R^3$-$3R^2$ coordinates, these Fe-rich

Table 8. Microprobe analyses of primary and secondary biotites from weakly kaolinized Chanon granite.

	Primary biotites				Secondary brown biotites				Secondary green biotites						
	1	2	3	4	1	2	3	4	5	6	7	8	9	10	11
Si	2.77	2.75	2.79	2.74	2.78	2.88	2.75	2.89	2.76	2.72	2.71	2.69	2.70	2.71	2.64
Al^{IV}	1.23	1.25	1.21	1.26	1.22	1.12	1.25	1.11	1.24	1.28	1.29	1.31	1.30	1.29	1.36
Al^{VI}	0.51	0.52	0.52	0.54	0.47	0.50	0.51	0.37	0.61	0.64	0.59	0.57	0.56	0.57	0.60
Mg	0.92	0.85	0.91	1.10	1.07	1.02	1.01	1.17	1.24	1.24	1.29	1.31	1.34	1.22	1.27
Fe^{2+}	1.18	1.19	1.16	1.10	1.17	1.07	1.20	1.13	1.00	0.97	0.94	1.02	0.97	1.03	1.00
Ti	0.14	0.15	0.14	0.07	0.09	0.10	0.08	0.09	0.01	0.01	0.01	0.01	0	0.02	0.01
Mn	0.03	0.03	0.03	0.02	0.03	0.04	0.02	0.03	0.02	0	0	0	0.02	0.02	0
Ca	0	0	0	0	0	0.01	0.01	0	0.01	0	0.01	0	0	0	0
Na	0.02	0.03	0.02	0.01	0.01	0	0.01	0.02	0.01	0.03	0.14	0	0.03	0.01	0.10
K	0.90	0.89	0.86	0.89	0.91	0.91	0.92	0.94	0.83	0.84	0.82	0.86	0.88	0.92	0.84
Σ oct	2.78	2.74	2.76	2.83	2.83	2.73	2.82	2.79	2.88	2.86	2.83	2.91	2.89	2.86	2.88

Calculated on the basis of 11 oxygens. Fe = Fe^{2+}.

chemical compositions are shifted towards the illite/montmorillonite or montmorillonite area (Table 13, Figure 10a; Veld, 1977, 1984, 1985).

In summary, the chemical composition of the I/S appears to have been influenced by the bulk rock chemistry. If it formed during the pervasive alteration, it contains only a small amount of phengitic substitutions (Mg + Fe ≤ 0.07 per half unit cell) and has mainly potassic interlayer charges in the albite-muscovite granite. In the Chanon granite the phengitic substitutions are greater (0.03 ≤ Mg + Fe ≤ 0.22), and the interlayer charges give greater Ca/(Ca + K) ratios. If it formed in veins, it shows similar differences in (Fe,Mg)-phengitic substitutions; it shows less phengitic substitution in the albite-muscovite granite and more in the Chanon granite, but the interlayer charges give more homogeneous and larger Ca/(Ca + K) ratios.

Biotite/vermiculite clay mineral

The biotite/vermiculite from the red, kaolinized Chanon granite yielded a 10.90-Å XRD reflection after the sample had been heated to 500°C. Microprobe analyses corresponded to a mixture of kaolinite and the mixed-layer material (Table 14). The iron oxides were of the goethite type. No smectite was identified in the kaolinitic and illitic matrix that replaced the plagioclase.

Table 9. Microprobe analyses of corrensite replacing biotites from weakly kaolinized Chanon granite.

Si	3.85	3.91	3.86	3.80	3.58	3.86	3.64	3.92
Al^{IV}	0.15	0.09	0.14	0.20	0.42	0.14	0.36	0.08
Al^{VI}	2.31	2.41	2.43	2.24	1.97	2.23	1.91	2.49
Mg	1.10	0.87	0.94	1.11	0.93	1.11	0.86	0.82
Fe	1.24	1.03	1.13	1.37	1.29	1.37	1.15	1.18
Ti	0.02	0.12	0.03	0.01	0.41	0.01	0.52	0.04
Mn	0.02	0.02	0.01	0.01	0.02	0.01	0.01	—
Ca	0.01	0.01	0.02	0.01	—	0.01	0.01	—
Na	0.02	0.08	0.02	0.07	0.02	—	—	0.01
K	0.37	0.41	0.51	0.38	0.37	0.43	0.51	0.45

Calculated on the basis of 14 oxygens. Fe = Fe^{2+}.

DISCUSSION

The petrographic observations suggest that the different secondary parageneses were first related in time to the formation of the greisen bodies, because of their broadly zoned patterns, and then to a massive hydrothermal alteration, which affected the granitic bodies. The chronological relations among the secondary minerals in veins and in pervasively altered zones of the Chanon and the albite-muscovite granites are summarized in Table 15.

Hydrothermal alteration related to greisen formation

The hydrothermal alteration in the albite-muscovite granite is relatively simple and corresponds typically to the greisen mineral assemblage of lepidolite + quartz. The hydrothermal alteration is more complex in the Chanon granite and is distributed zonally around the greisen itself. This greisen is composed chiefly of tourmaline; trilithionite, which replaces primary biotite; and lepidolite, which invades muscovite, feldspar, and quartz.

Crystallographic properties and chemical compositions of Li-rich micas have been determined on both natural and synthetic minerals (Robert and Volfinger, 1979; Munoz, 1968, 1971; Foster, 1960; Rieder, 1971; Monier, 1985). Li-rich micas can be considered to be a solid solution between normal non-Li-bearing dioctahedral or trioctahedral micas and Li-rich micas

Table 10. Microprobe analyses from fresh albite-muscovite granite.

SiO_2	45.48	43.45	45.92	40.55	45.99
Al_2O_3	36.41	39.13	37.63	32.43	34.62
Fe_2O_3	0.32	0.37	0.52	0.47	0.10
MnO	0.07	—	—	0.17	1.17
MgO	—	0.08	0.26	0.25	0.27
TiO_2	—	0.03	0.31	—	—
CaO	0.02	0.21	0.38	0.38	0.37
K_2O	1.35	1.07	2.49	2.23	2.55
Na_2O	0.13	0.24	0.29	0.30	0.50

https://doi.org/10.1346/CCMN.1988.0360604 Published online by Cambridge University Press

Table 11. Microprobe analyses of illite-kaolinite-illite/smectite assemblage crystallizing in the albite-muscovite granite and its greisen facies.

	Albite-muscovite granite						Greisen						
Si	3.00	3.00	3.08	3.10	3.01	3.09	3.18	3.20	3.13	3.21	3.21	3.25	3.20
Al^{IV}	1.00	1.00	0.92	0.90	0.99	0.91	0.82	0.80	0.87	0.79	0.79	0.75	0.80
Al^{VI}	2.15	2.11	2.02	2.01	2.13	1.99	1.95	1.99	2.06	2.06	2.07	2.13	2.12
Mg	0.02	0.01	0.06	—	0.03	—	—	—	—	—	—	—	—
Fe	—	0.02	0.01	0.00	0.01	0.02	—	0.01	0.01	0.02	0.03	0.01	0.02
Ti	—	0.01	—	—	0.01	0.01	—	—	—	—	—	—	—
Mn	—	—	0.01	—	—	0.01	—	—	0.01	0.01	0.01	—	0.01
Ca	—	—	0.02	—	0.02	—	—	—	—	—	—	0.01	—
Na	0.05	0.04	0.08	0.01	0.04	0.05	0.05	0.01	0.06	—	0.06	0.02	0.03
K	0.43	0.51	0.55	0.81	0.41	0.81	0.82	0.76	0.62	0.56	0.43	0.29	0.33
Σ oct	2.17	2.15	2.10	2.01	2.18	2.03	1.95	2.00	2.08	2.09	2.11	2.14	2.15

Calculated on the basis of 11 oxygens. Fe = Fe^{2+}.

(e.g., polylithionite, trilithionite, taeniolite). Li-rich micas crystallize in bodies similar to greisens at temperatures >400°C (Kükne *et al.*, 1972; Rieder *et al.*, 1970; Charoy, 1979). The XRD patterns of the trilithionites analyzed from the Montebras cupola indicate that this lithian phase approximates a phlogopite 35%-trilithionite 65% solid solution (Robert and Volfinger, 1979; Monier, 1985).

In the nearer alteration zone surrounding the greisen itself and the greisen veins, primary biotite has apparently recrystallized to secondary brown biotite, which is richer in Mg and depleted in Ti. These reactions are similar to those surmised for the potassic alteration zones in porphyry copper environments and indicate a high-temperature hydrothermal process (400°–450°C) (Jacobs and Parry, 1976, 1979; Nielsen, 1968; Beane, 1974; Fournier, 1967).

The farther alteration zone surrounding the greisen is characterized by coexisting phengite-green biotite. The white mica has a low interlayer charge (0.68–0.96), and the biotite has a composition that ranges towards Al-phlogopite. Similar chemical shifts in porphyry copper environments have been attributed to a temperature decrease (Jacobs and Parry, 1979; Beaufort, 1984). The crystallization temperature of the phengite-Al-phlogopite assemblage was estimated by these authors to be at least 300°C in such environments and >350°C in active geothermal fields; a corrensite-chlorite-orthoclase assemblage has been reported to form between 300° and 220°C (MacDowell and Elders, 1980). Around the greisen veins corrensite crystallized in the farther alteration zone. According to Velde (1977, 1984, 1985), the thermal stability of corrensite ranges from 180°–200° to 280°C.

Tosudite and kaolinite coexist in the fresh albite-muscovite granite. The tosudite is an intermediate alteration phase, forming after the micaceous phases and before the I/S (Matsuda and Henmi, 1973). It probably crystallized from a circulating hydrothermal solution containing high Al and low Li contents and of pH 4–6 (Maksimović and Brindley, 1980; Nishiyama *et al.*, 1975). In the Montebras cupola, tosudite apparently crystallized at lower temperature than any other Li-rich phase.

Late hydrothermal event

Random I/S coexists with illite and/or kaolinite in the pervasive alteration zone of the albite-muscovite granite and in vein fillings in both granite bodies. In the pervasive alteration zone, this assemblage replaces

Table 12. Microprobe analyses of illite-kaolinite-illite/smectite assemblage pseudomorphosing after primary minerals in Chanon granite.

Si	3.27	3.21	3.14	3.24	3.19	3.15	3.31	3.40	3.30	3.26
Al^{IV}	0.73	0.79	0.86	0.76	0.81	0.85	0.69	0.60	0.70	0.74
Al^{VI}	1.84	1.91	2.00	1.90	2.09	2.12	2.14	2.08	2.14	2.04
Mg	0.04	0.03	0.05	0.12	0.07	0.03	—	—	—	0.01
Fe	0.07	0.08	0.05	0.10	0.04	0.07	0.04	0.07	0.03	0.18
Ti	0.03	0.02	—	—	—	—	—	—	—	0.01
Mn	—	—	—	—	—	0.01	—	—	0.01	—
Ca	—	—	—	0.01	0.01	0.01	0.02	0.02	0.03	0.03
Na	0.14	—	—	—	—	0.01	—	0.04	—	0.03
K	0.86	0.76	0.69	0.69	0.44	0.25	0.14	0.15	0.11	0.08
Σ oct	1.98	2.04	2.10	2.12	2.20	2.23	2.18	2.15	2.18	2.24

Calculated on the basis of 11 oxygens. Fe = Fe^{2+}.

https://doi.org/10.1346/CCMN.1988.0360604 Published online by Cambridge University Press

Table 13. Average microprobe analyses of six veinlet fillings cutting previously altered Chanon granite (1, 2, 3) and albite-muscovite granite (4, 5, 6).

	1	2	3	4	5	6
Si	3.79	3.39	3.50	3.38	3.37	3.13
Al^{IV}	0.21	0.61	0.50	0.62	0.63	0.87
Al^{VI}	1.60	1.89	1.68	1.82	1.77	1.62
Mg	0.12	0.06	0.18	0.02	0.06	0.07
Fe	0.41	0.26	0.23	0.12	0.11	0.15
Ti	0.02	0.01	—	0.03	0.03	0.22
Mn	—	—	—	—	—	—
Ca	0.14	0.08	0.14	0.08	0.15	0.26
Na	—	—	0.08	—	0.07	—
K	0.04	0.08	0.29	0.48	0.51	0.19
Σ oct	2.01	2.16	2.09	2.04	1.96	2.06

1 = pure smectite; 2–6 = illite/smectite (40–50% smectite layers)-illite-kaolinite assemblages. Calculated on the basis of 11 oxygens. Fe = Fe^{2+}.

primary micas and feldspars in the fresh albite-muscovite granite and micaceous phases in the greisen. The I/S contains 40% smectite layers and has potassic interlayer cations and very limited Al/Fe-Mg octahedral substitutions. In the two granites, the I/S filling the late veinlets contains 40 to 100% smectite layers. The smectite layers contain Mg and Ca as interlayer cations and have extensive Al/Fe-Mg octahedral substitutions.

The random nature of the I/S implies temperature conditions of <100°C (Velde, 1977, 1984, 1985; Eberl and Hower, 1977). Similar low-temperature hydrothermal assemblages have been described in granite and syenite alteration zones (Meunier and Velde, 1982; Meunier, 1982; Beaufort and Meunier, 1983a, 1983b).

Weathering

In the red, kaolinized, friable Chanon granite, biotite has broken down into vermiculite-kaolinite assemblages and iron oxides. In the albite-muscovite granite, in the absence of a primary Fe-Mg phase, such as biotite, the detrital kaolinite-iron oxide deposits observed appear to have been derived from the overlying, weathered Chanon granite.

In granitic rocks, more than 75% of the interlayer sites of hydrothermal smectites are filled with K (Cathelineau, 1982), whereas smectites in weathering zones contain Mg and Ca as interlayer cations (Meunier, 1980). The kaolinite-vermiculite and iron oxide assemblage is characteristic of weathering in a temperate climate (Meunier, 1980). Noncrystalline iron oxides or goethite were not noted in earlier hydrothermal alteration zones. On the other hand, the potassic smectites or potassic I/S were not noted in weathering zones in which vein-filling I/S contains Ca and Mg as interlayer cations and in which the pure smectite has a Ca-Mg-montmorillonite composition. The potassic smectites seem to have been obliterated by weathering.

SUMMARY AND CONCLUSION

The chemical evolution of circulating hydrothermal solutions can be inferred from the nature of the alteration parageneses found in the two granite bodies (Figures 11a and 11b and Table 15).

Magmatic stage

The first alteration event was magmatic albitization; both the albite-muscovite granite and the Chanon granite were apparently affected by high temperature and K-Li-F-rich fluids (Charoy, 1979). The high fluid/rock ratio induced the obliteration of all primary minerals. The K, Li, F, and OH^- from the hydrothermal solution were apparently incorporated in the lithian micas that characterize the formation of the greisen. In the Chanon granite, primary biotite was replaced by trilithionite and lepidolite, giving rise to an increase in the concentration of Mg in the solution. During the late cooling stages, a decrease of the temperature and the fluid/rock ratio induced a progressive removal of Mg from solution, and secondary, brown biotite crystallized. The brown biotite was followed by green biotite and phengite as long as the K activity remained sufficiently high. In the farther alteration zone, which surrounds the greisen veinlets, the occurrence of cor-

Table 14. Microprobe analyses of cryptocrystalline kaolinite-goethite deposits in voids of quartzitic facies within albite-muscovite granite and of kaolinized biotite in red, kaolinized facies of Chanon granite.

	Cryptocristalline deposit in albite-muscovite granite						Kaolinized biotites from Chanon granite							
Si	3.59	3.36	3.33	3.29	3.62	3.26	2.87	3.04	3.12	2.98	2.99	3.12	3.19	3.10
Al^{IV}	0.49	0.64	0.67	0.71	0.38	0.74	1.13	0.96	0.88	1.02	1.01	0.88	0.81	0.90
Al^{VI}	1.77	1.84	1.89	1.85	1.80	2.21	0.71	1.28	2.04	1.44	1.86	2.04	2.21	2.20
Mg	0.01	0.02	0.01	0.04	0.04	—	1.10	0.62	0.06	0.41	0.25	0.10	0.02	0.06
Fe	0.35	0.32	0.26	0.30	0.13	0.01	0.93	0.50	0.06	0.58	0.29	0.20	0.53	0.13
Ti	0.04	0.04	0.03	0.04	—	—	0.05	0.03	0.01	0.07	0.02	—	—	—
Mn	—	—	—	0.01	0.03	—	0.02	0.02	0.01	—	—	—	—	—
Ca	0.04	0.04	0.03	0.03	0.02	—	0.01	0.01	—	0.02	0.01	0.08	—	0.01
Na	0.01	0.01	0.03	0.06	0.05	0.04	0.01	0.01	0.02	—	—	—	—	—
K	0.22	0.22	0.24	0.20	0.51	0.33	0.70	0.39	0.44	0.40	0.24	0.10	0.03	0.02
Σ oct	2.14	2.22	2.19	2.24	2.00	2.22	2.81	2.45	2.18	2.50	2.42	2.34	2.76	2.39

Calculated on the basis of 11 oxygens. Fe = Fe^{2+}.

https://doi.org/10.1346/CCMN.1988.0360604 Published online by Cambridge University Press

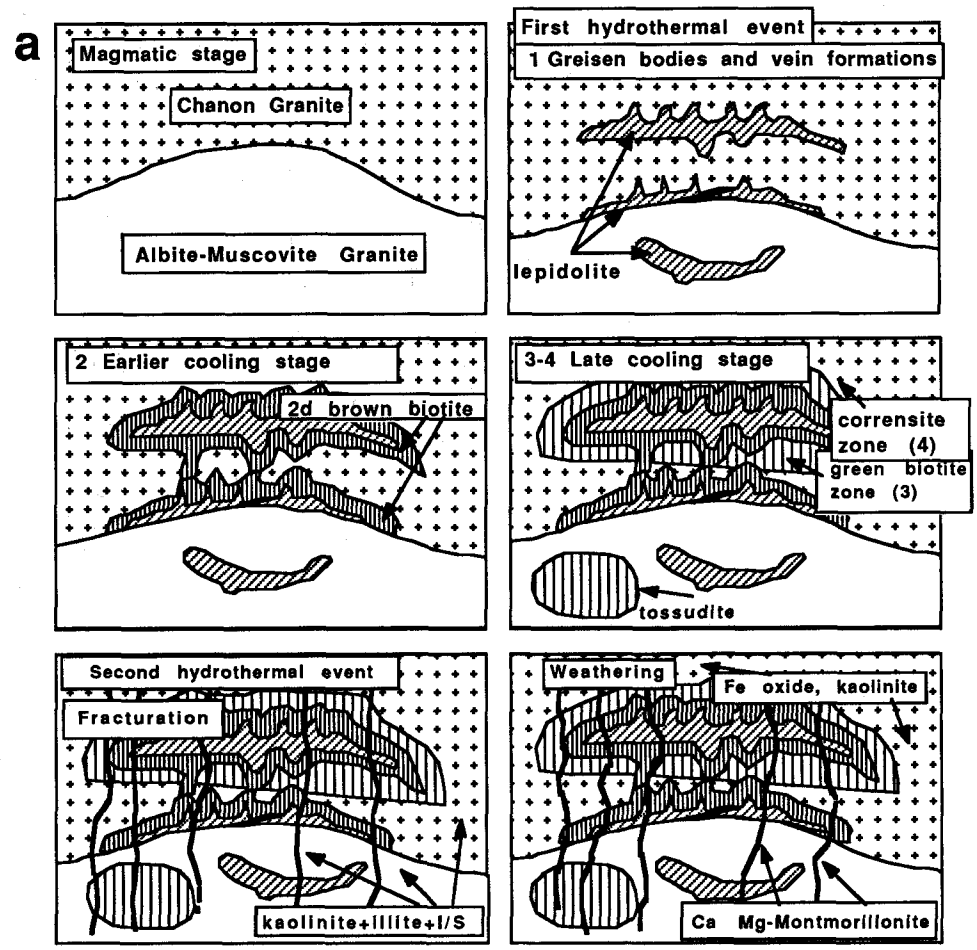

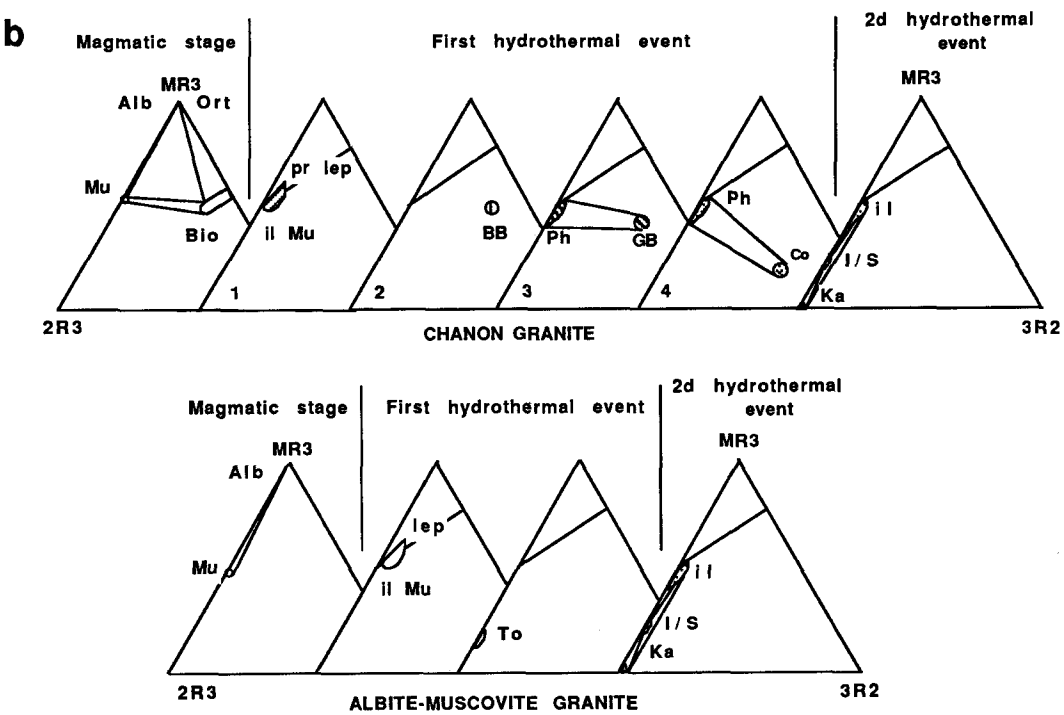

https://doi.org/10.1346/CCMN.1988.0360604 Published online by Cambridge University Press

Table 15. Alteration facies and associated alteration parageneses observed in albite muscovite-granite and Chanon granite.[1]

Petrographic facies	Pervasive alteration	Veins	Alteration episodes
	Albite-muscovite granite		
Greisen	**1** lepidolite-quartz		first hydrothermal episode
Weakly kaolinized albite-muscovite-granite			
Chloritic alteration	**3** tosudite-kaolinite		
Argillic alteration	**4** illite-kaolinite-I/S	illite-kaolinite-I/S	late hydrothermal episode
		kaolinite + Fe oxides	weathering
	Chanon granite		
Greisen facies	**1** lepidolite, trilithionite, quartz, tourmaline	lepidolite, trilithionite, quartz, tourmaline	first hydrothermal episode
Nearer surrounding zone	**2** secondary brown biotites	secondary brown biotites	
Farther surrounding zone	**3** green biotites, phengites	**4** corrensite, phengite	
White weakly kaolinized granite	kaolinite, illite	kaolinite, illite, I/S	late hydrothermal episode
Red kaolinized granite	kaolinite, goethite, biotite/vermiculite	kaolinite, illite, Ca-Mg-smectite	weathering

[1] Boldface numbers refer to alteration episodes sketched in Figures 11a and 11b.

rensite characterizes a late cooling stage, accompanied by a decrease in the activities of K and Mg. Here, the Si activity increased sufficiently to allow the crystallization of smectitic layers in I/S. In a similar range of temperature and in the absence of Fe-Mg-rich phases in the albite-muscovite granite, a decrease of the K activity and an increase of the Si activity allowed Li-bearing tosudite to crystallize in this aluminous medium. The tosudite trapped the Li in its chloritic layers (cookeite type).

The second hydrothermal event affected the granite bodies at lower temperature. The alteration assemblage is illite + I/S + kaolinite. K and Mg, released from recrystallized biotite and muscovite, were trapped in the potassic interlayers and in the Al → Mg octahedral substitutions of illites and I/S, respectively. With a decrease of temperature and fluid-rock interaction, the K activity decreased, whereas the Si activity in solution increased. Newly formed clay minerals are characterized by low K and high Si contents; the mineral assemblage is closed to the kaolinite pole in the MR^3-$2R^3$-$3R^2$ diagram. In the albite-muscovite granite the secondary phases were depleted in Fe and Mg because of the lack of primary Fe, Mg-rich minerals, demonstrating the lack of chemical exchange between the two granitic bodies during the hydrothermal events.

Weathering

Weathering pervasively altered the Chanon granite, which overlies the albite-muscovite granite. In the Chanon granite, primary biotite, secondary biotite, and plagioclase were altered to kaolinite. As a result, weathering solutions were enriched in Fe, Mg, and Ca. The albite-muscovite granite is mainly characterized by the lack of phases susceptible to weathering; only local detrital deposits (kaolinite and Fe oxides) inherited from the weathered Chanon granite are present in voids. Fe-, Mg-, and Ca-rich solutions appear to have percolated through the two granitic bodies in subvertical cracks and crystallized Ca-Mg-montmorillonite, which obliterated the hydrothermal potassic smectites.

REFERENCES

Aubert, G. (1969) Les coupoles granitiques de Montebras et d'Echassières (Massif Central français) et la genèse de leur minéralisation étain-lithium-tungstène-béryllium: *Mém. BRGM* **46**, 354 pp.

Beane, R. E. (1974) Biotite stability in the porphyry copper environment: *Econ. Geol.* **69**, 241–256.

Beaufort, D. (1981) Etude pétrographique des altérations hydrothermales superposées dans le porphyre cuprifère de Sibert (Rhône, France). Influence des microsystèmes géochimiques dans la différenciation des micas blancs et des phases trioctaédriques: Thèse 3e cycle, Univ. Poitiers, Poitiers, France, 147 pp.

←

Figure 11. (a) Sketch of hydrothermal events, successive cooling stages, and weathering which have affected the two granite bodies of the Montebras cupola. (b) Representation of the successive alteration parageneses in MR^3-$2R^3$-$3R^2$ coordinates (Table 15).

https://doi.org/10.1346/CCMN.1988.0360604 Published online by Cambridge University Press

Beaufort, D. (1984) An interstratified illite/smectite mineral from the hydrothermal deposit in Sibert, Rhône, France: *Clays & Clay Minerals* **32,** 154–156.

Beaufort, D. and Meunier, A. (1983a) A petrographic study of phyllic alteration superimposed on potassic alteration: The Sibert porphyry deposit (Rhône, France): *Econ. Geol.* **78,** 1514–1527.

Beaufort, D. and Meunier, A. (1983b) Petrographic characterization of an argillic hydrothermal alteration containing illite, K-rectorite, K-beidellite, kaolinite and carbonates in a cupromolybdenic porphyry at Sibert (Rhône, France): *Bull. Minér.* **106,** 533–551.

Beaufort, D., Dudoignon, P., Proust, D., Parneix, J. C., and Meunier, A. (1983) Microdrilling in thin section: A useful method for identification of clay minerals *in situ*: *Clay Miner.* **18,** 219–222.

Brindley, G. M. and Brown, G., eds. (1980) *Crystal Structures of Clay Minerals and their X-Ray Identification:* Mineralogical Society, London, 495 pp.

Cathelineau, M. (1982) Les gisements d'uranium liés spatialement aux leucogranites Sud-armoricains et leur encaissant métamorphique: Relation et interaction entre les minéralisations et divers contextes géologiques et structuraux: *Sci. de la Terre* **42,** 375 pp.

Charoy, B. (1975) Ploëmeur kaolin deposit: An example of hydrothermal alteration: *Petrology I,* **4,** 253–266.

Charoy, B. (1979) Définition et importance des phénomènes deutériques et des fluides associés dans les granites. Conséquences métallogéniques: *Mém. BRGM* **37,** 364 pp.

Creach, M., Meunier, A., and Beaufort, D. (1986) Tosudite occurrence in the kaolinized granitic cupola of Montebras (Creuse, France): *Clay Miner.* **21,** 225–230.

Dudoignon, P. (1983) Altérations hydrothermales et supergènes des granites. Etude des gisements de Montebras (Creuse), de Sourches deux-Sèvres) et des arènes granitiques (Massif de Parthenay): Thèse 3e cycle Univ. Poitiers, Poitiers, France, 120 pp.

Eberl, D. and Hower, J. (1977) The hydrothermal transformation of sodium and potassium smectite into mixed layer clay: *Clays & Clay Minerals* **25,** 215–227.

Exley, C. S. (1976) Observations on the formation of kaolinite in the St-Austell granite, Cornwall: *Clay Miner.* **11,** 51–63.

Foster, M. D. (1960) Interpretation of the compositions of lithium micas: *U.S. Geol. Surv. Prof. Pap.* **354,** 115–146.

Fournier, R. O. (1967) The porphyry copper deposit exposed in the Liberty open pit-mine near Ely, Nevada, Part. II. The formation of hydrothermal alteration zones: *Econ. Geol.* **62,** 207–227.

Ichikawa, A. and Shimoda, S. (1976) Tosudite from the Hokuno mine, Hokuno, Gifu Prefecture, Japan: *Clays & Clay Minerals* **24,** 142–148.

Jacobs, D. C. and Parry, W. T. (1976) A comparison of the geochemistry of biotite from some Basin and Range stocks: *Econ. Geol.* **71,** 1029–1035.

Jacobs, D. C. and Parry, W. T. (1979) Geochemistry of biotite in the Santa Rita porphyry copper deposit, New Mexico: *Econ. Geol.* **74,** 860–887.

Konta, J. (1969) Comparison of the proofs of hydrothermal and supergene kaolinization in two areas of Europe: in *Proc. Int. Clay Conf., Tokyo, 1969, Vol. 1,* L. Heller, ed., Israel Univ. Press, Jerusalem, 281–290.

Kükne, R., Wasternack, J., and Schulze, C. (1972) Postmagmatische Metasomatose Evokontakt der Jüngeren post kinematischen Granite des Erzgebirges: *Geologie Dtsch.* **21,** 494–520.

MacDowell, D. M. C. and Elders, W. A. (1980) Authigenetic layer silicate in borehole Elmore 1, Salton Sea geothermal field, California, U.S.A.: *Contrib. Mineral. Petrol.* **74,** 293–310.

Maksimović, Z. and Brindley, G. W. (1980) Hydrothermal alteration of a serpentine near Takovo, Yugoslavia, to chromium bearing illite/smectite, kaolinite, tosudite, and halloysite: *Clays & Clay Minerals* **28,** 295–302.

Matsuda, T. and Henmi, K. (1973) Hydrothermal behavior of the interstratified mineral from the mine of Ebara, Hyago Prefecture, Japan (an example of changes from randomly interstratified clay mineral to regular one): *J. Clay Science Soc. Japan* **13,** 87–94.

Meunier, A. (1980) Les mécanismes de l'altération des granites et le rôles des microsystèmes. Etude des arènes du massif granitique de Parthenay (Deux-Sèvres): *Mém. Soc. Géol. Fr.* **140,** 80 pp.

Meunier, A. (1982) Superposition de deux altérations hydrothermales dans la syénite monzonitique du Bac-de Montmeyre (sondage INAG 1, Massif Central, France): *Bull. Minéral.* **105,** 386–394.

Meunier, A. and Velde, B. (1982) Phengitization, sericitization and potassium beidellite in a hydrothermally altered granite: *Clay Miner.* **17,** 285–299.

Monier, G. (1985) Cristallochimie des micas des leucogranites. Nouvelles données expérimentales et applications pétrologiques: Thèse Doctorat ès sciences, Univ. Orléans, Orléans, France, 299 pp.

Munoz, J. L. (1968) Physical properties of synthetic lepidolites: *Amer. Mineral.* **56,** 1490–1512.

Munoz, J. L. (1971) Hydrothermal stability relations of synthetic lepidolite: *Amer. Mineral.* **56,** 2069–2087.

Nicolas, J. and Rosen, A. (1966) Le massif des Colettes (Allier) et ses minéralisations: *Bull. Soc. Fran. Mineral. Crist.* **7,** 126–128.

Nielsen, R. L. (1968) Hypogene texture and mineral zoning in a copper-bearing granodiorite porphyry stock, Santa Rita, New Mexico: *Econ. Geol.* **63,** 37–50.

Nishiyama, T., Shimoda, S., Shimosaka, K., and Kanaoka, S. (1975) Lithium-bearing tosudite: *Clays & Clay Minerals* **23,** 337–342.

Reynolds, R. C. (1980) Interstratified clay minerals: in *Crystal Structure of Clay Minerals and their X-ray Identification,* G. W. Brindley and G. Brown, eds., Mineralogical Society, London, 249–303.

Reynolds, R. C. and Hower, J. (1970) The nature of interlaying in mixed-layer illite-montmorillonite: *Clay & Clay Minerals* **18,** 25–36.

Rieder, M. (1971) Stability and physical properties of synthetic lithium-iron micas: *Amer. Mineral.* **56,** 256–280.

Rieder, M., Huka, M., Kucerova, D., Minarik, L., Obermajor, J., and Povondra, P. (1970) Chemical composition and physical properties of lithium-iron micas from the Krusne Hory Mts. (Erzgebirge): *Contrib. Mineral. Petrol.* **27,** 131–158.

Robert, J. L. and Volfinger, M. (1979) Etude expérimentale de lépidolites trioctaédriques hydroxylées: *Bull. Minéral.* **102,** 21–25.

Shimoda, S. (1975) X-Ray and I.R. studies of sudoite and tosudite: *Contrib. Clays Min. in Honor Prof. Tushio Sudo,* 92–96.

Sudo, T. and Shimoda, S. (1978) *Clays and Clay Minerals of Japan:* Elsevier, Amsterdam, 325 pp.

Velde, B. (1977) *Clays and Clay Minerals in Natural and Synthetic Systems:* Elsevier, Amsterdam, 218 pp.

Velde, B. (1984) Electron microprobe analysis of clay minerals: *Clay Miner.* **19,** 243–247.

Velde, B. (1985) *Clay Minerals. A Physico-Chemical Explanation of their Occurrence:* Elsevier, Amsterdam, 427 pp.

(Received 3 November 1987; accepted 22 June 1988; Ms. 1730)